ACS APPLIED NANO MATERIALS
Cite This: ACS Appl. Nano Mater. 2019, 2, 1185−1193
Article
www.acsanm.org

Solid-State Encapsulation and Color Tuning in Films of Cesium Lead Halide Perovskite Nanocrystals for White Light Generation

Ilker Torun,[†] Yemliha Altintas,[‡] Ahmet Faruk Yazici,[‡] Evren Mutlugun,*[,§,∥] and M. Serdar Onses*[,†,∥]

[†]Department of Materials Science and Engineering, Nanotechnology Research Center (ERNAM) Erciyes University, Kayseri 38039, Turkey

[‡]Department of Materials Science and Nanotechnology Engineering and [§]Department of Electrical and Electronics Engineering, Abdullah Gul University, Kayseri 38080, Turkey

[∥]UNAM − Institute of Materials Science and Nanotechnology, Bilkent University, Ankara 06800, Turkey

Supporting Information

ABSTRACT: Perovskite nanocrystals (PNCs) are highly demanding nanomaterials for solid-state lighting applications. A challenge for their exploitation in practical applications is the insufficient ambient and water stability associated with their ionic nature. Here we report a novel route for solid-state encapsulation of films of perovskite nanocrystals (PNCs) through vapor-phase deposition of a thin and hydrophobic layer of fluoroalkyltrichlorosilanes (FAS). High quality nanoscale crystals of $CsPbBr_3$ were synthesized with well-established colloidal methods and coated on solid substrates. The films of PNCs were then subjected to vapor of FAS for short durations of time (<60 s) in ambient atmosphere, resulting in deposition of a thin (<20 nm) hydrophobic layer. Besides providing a barrier for water and humidity, the vapor-phase deposition of FAS was accompanied by the blue shift of the emission wavelength of the PNCs. The color shift results from the partial exchange of Br with Cl anions, which emerge during the self-hydrolysis of the silane molecules. Throughout this process, we demonstrate the enhanced water stability of the films of PNCs and fine tunability of the wavelength in films from 516 nm to 488 nm. The fabrication of a white-light-emitting diode and tunability of the color coordinates with the duration of the FAS deposition were demonstrated. The rapid, scalable, and inexpensive solid-state encapsulation approach shows great promise for films of halide perovskites.

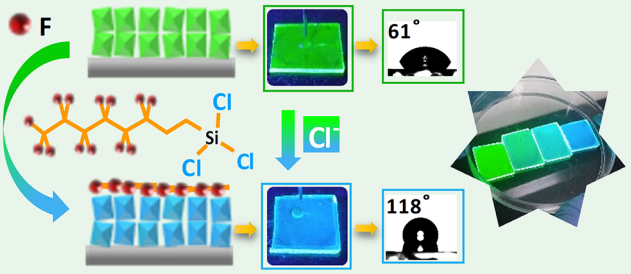

KEYWORDS: *perovskite nanocrystals, silanes, vapor-phase deposition, colloidal optoelectronics*

1. INTRODUCTION

Nanoscale crystals of lead halide perovskites present highly efficient, versatile, low-cost, and solution-processable routes for fabrication of white-light-emitting diodes.[1] Inspired by the great success in thin films of organo-lead halide perovskites ($CH_3NH_3PbX_3$, X = Cl, Br, I) for photovoltaics,[2] colloidal forms of such materials have recently attracted an immediate interest. Following the initial studies on the hybrid organic−inorganic ones,[3,4] colloidal synthesis of all inorganic cesium lead halide ($CsPbX_3$) perovskite nanocrystals (PNCs) has enabled solution-processing-based preparation of materials with extremely interesting optical properties.[5] Their high photoluminescence quantum yields exceeding 90%,[6] wide tunability of the color,[7] narrow emission bandwidths,[8] and large optical absorption cross section[9] warrant their highly promising position for light-emitting applications. In comparison to conventional quantum dots based on group II−VI and III−V elements (e.g., CdSe and InP), PNCs offered enhanced tolerance to the variations in the size of the nanocrystals and surface defects associated with the dangling bonds.[10] The size tolerance, for instance, allowed for strong photoluminescence at length scales larger than the excitonic Bohr diameter of the material.[7] These characteristics established the foundations for the fabrication of light-emitting diodes (LEDs),[11] lasers,[12] solar cells,[13] and photodetectors[14] based on all inorganic lead halide perovskites. Further advancing the capabilities of PNCs in practical applications requires careful interpretation of the stability and color tunability.

The ionic nature of all inorganic PNCs results in high levels of susceptibility to polar solvents and moisture.[15] The stability of PNCs is of significant importance to enable practical applications based on these interesting materials. A range of different strategies has been recently reported to overcome this issue. Rogach and co-workers[16] have demonstrated that the stability of inorganic PNCs against water could be significantly improved by coating the surface of nanoparticles with polyhedral oligomeric silsesquioxane. This coating enabled highly stable aqueous solutions and white light-emitting diodes

Received: November 10, 2018
Accepted: January 30, 2019
Published: January 30, 2019

DOI: 10.1021/acsanm.8b02030
ACS Appl. Nano Mater. 2019, 2, 1185−1193

using mixtures of red and green emitting nanocrystals without anion-exchange reactions. The encapsulation with different forms of silica has proved to be a highly effective strategy to improve the stability of PNCs. One strategy[17,18] involved addition of (3-aminopropyl)triethoxysilane into the precursor solution to serve as a capping agent and protection layer. Besides the role of amine headgroup in the dissolution of precursors and passivation of the surface, silyl ether groups can polymerize in the presence of moisture to form a protection layer that is composed of silica. This protection layer prevented anion exchange and significantly improved the air stability of the all inorganic PNCs. The encapsulation with polymeric materials is another strategy that has been utilized to improve the stability. For this purpose, PNCs were incorporated within electrospun nanofibers,[19] thin films[20] of polymer and block copolymer micelles,[21] and polystyrene spheres.[22] Other approaches included exposure of films of PNCs to X-rays,[23] incorporation of PNCs into mesoporous silica nanoparticles,[24] anchoring of PNCs to the surface of silica particles,[25] increasing the iodine content of the surface,[26] decoration of the surface of the nanocrystals with ZnS,[27] and using different ligands.[28] These approaches mostly focused on encapsulating individual PNCs and required additional and tedious processing steps. It remains intact to develop simple, versatile, and rapid approaches for direct encapsulation of the as-synthesized PNCs after deposition of the films.

The anion-exchange-mediated postsynthesis color engineering is a unique capability presented by PNCs. The type and ratio of the halide anions (Cl, Br, I) determine the photoluminescence wavelength of these nanomaterials. The complete anion exchange from Cl to Br and Br to I results in change of the color from blue to green and green to red, respectively.[29] Furthermore, the partial exchange of anions allows for precise tuning of the emission wavelength throughout the entire visible region.[30] A remarkable feature is that the size and shape of the nanocrystals can be retained during these anion-exchange reactions. Recent reports have shown that anion-exchange reactions can also be performed in the vapor phase. Manna and co-workers[23] used hydrohalic vapors for conversion in between $CsPbBr_3$ and $CsPbCl_3$ nanocrystals to fabricate patterned arrays of PNCs. The ability to tune the color of PNCs with hydrochloric acid vapor was employed to construct a hydrochloric acid sensor.[31] Such vapor-phase anion-exchange reactions allowed for tuning the microstructure of thin films of organometal halide perovskites to increase the power conversion efficiency of solar cells.[32] These studies showed the promise of vapor-phase anion exchange reactions for dynamically tuning the color of films of PNCs. Development of vapor-phase postdeposition strategies that simultaneously enable encapsulation of PNCs and tuning of their emission color will provide substantial capabilities in colloidal optoelectronics applications.

To address the above-mentioned issues, in this work we propose the vapor-phase encapsulation of PNCs with a simple approach using fluoroalkyltrichlorosilanes (FAS) to efficiently provide stability as well as to demonstrate an effective tuning of white color coordinates of a fabricated hybrid light-emitting diode. The encapsulation process is simply performed by placing a substrate with a film of PNCs and a droplet of FAS in a closed container for tens of seconds. A unique aspect of our approach is that the deposition of a hydrophobic film is accompanied by a change in the emission color. The release of hydrochloric acid during self-hydrolysis of the silane mediates the partial exchange of bromine anions with chlorine anions, resulting in a blue shift of the emission wavelength of the PNCs. Effects of the deposition time and environment on the thickness and wetting behavior of the films of FAS and emission wavelength of the PNC film are systematically studied. The deposition of FAS renders the surface of the films hydrophobic and improves their water stability. When performed with films of $CsPbBr_3$ nanocrystals, the deposition of FAS results in the change of the emission color from green to blue due to the shift of the composition to $CsPbBr_{3-x}Cl_x$. We finally fabricate down-conversion white-light-emitting diodes based on PNC films and show that the Commission Internationale de l'Eclairage (CIE) color coordinates can be modulated with the duration of FAS deposition. Although conventional nanocrystal hybrid LEDs necessitate choosing the red and green emitters before hybridization (in the dispersion mode), our approach allows for continuous color tunability for green PNC emitters as real time on the chip level therefore presents a novel proof-of-concept approach for color tuning of the white coordinate as desired.

2. EXPERIMENTAL SECTION

2.1. Materials. Octadecene (90%), oleic acid (90%), oleylamine (70%), Cs_2CO_3 (99.99%), $PbBr_2$ (99.999), and hexane (99%) were utilized as received from Sigma-Aldrich. Silicon wafers (⟨100⟩) and glass slides were purchased from Wafer World Inc. and Isolab Inc., respectively. Tridecafluoroalkyl-1,1,2,2-tetrahydrooctyltrichlorosilane was purchased from Gelest Inc. and referred to as FAS.

2.2. Synthesis of Perovskite Nanocrystals. Cs-oleate precursor was prepared according to the following recipe. Octadecene (ODE, 20 mL), Cs_2CO_3 (0.4 g), and oleic acid (OA, 1.55 mL) were mixed in a three-necked flask and stirred under vacuum at 120 °C for 60 min. The temperature of the solution was increased to 150 °C and kept at this temperature until complete dissolution of the entire Cs_2CO_3 in ODE.

$CsPbBr_3$ PNCs were synthesized with a slight modification of the recipes reported in the previous studies.[5,33] 0.138 mg of $PbBr_2$ and 7.5 mL of ODE were mixed in a 25 mL flask and subjected to vacuum at room temperature for 30 min, followed by stirring under an argon gas atmosphere at 120 °C. One milliliter of oleylamine and 1 mL of OA were added into the solution and kept for 10 min at 120 °C. Afterward, the temperature of the solution was raised to 180 °C, and 0.8 mL of Cs-oleate was injected swiftly into the solution, which was then cooled to room temperature within 5 s. As-synthesized PNCs were purified following our recent study[34] by doubling the amount of the solvent.

2.3. Deposition of Perovskite Nanocrystal Films. Silicon and glass substrates (1×1 cm^2) were washed under sonication in acetone and ethanol for 5 min each and then dried with nitrogen. The substrates were then subjected to UV-ozone cleaning (Bioforce, procleaner) for 20 min. To suppress the formation of coffee-ring effects, the substrates were hydrophobized through vapor-phase deposition (see details in the following section) of a film of FAS for 30 s. The films of the nanocrystals were deposited on the hydrophobized substrate by spotting a 10 μL drop of PNCs dispersed in hexane at a concentration of 30 mg/mL.

2.4. Vapor-Phase Postdeposition of FAS. Three different types of substrates (1×1 cm^2) were used for vapor-phase deposition of FAS: (i) the freshly cleaned bare silicon substrates for monitoring the thickness of the deposited film; (ii) PNC films deposited on the silicon/glass substrates as described in the preceding section; (iii) gold films with a thickness of 100 nm deposited on the freshly cleaned silicon substrates by thermal evaporation (Nanovak NVTS-500) at a pressure $<5 \times 10^{-6}$ Torr with a deposition rate of 0.04 nm/s. In all cases, cleaning of the substrates was performed by washing under sonication in acetone and ethanol for 5 min each followed by drying

DOI: 10.1021/acsanm.8b02030
ACS Appl. Nano Mater. 2019, 2, 1185−1193

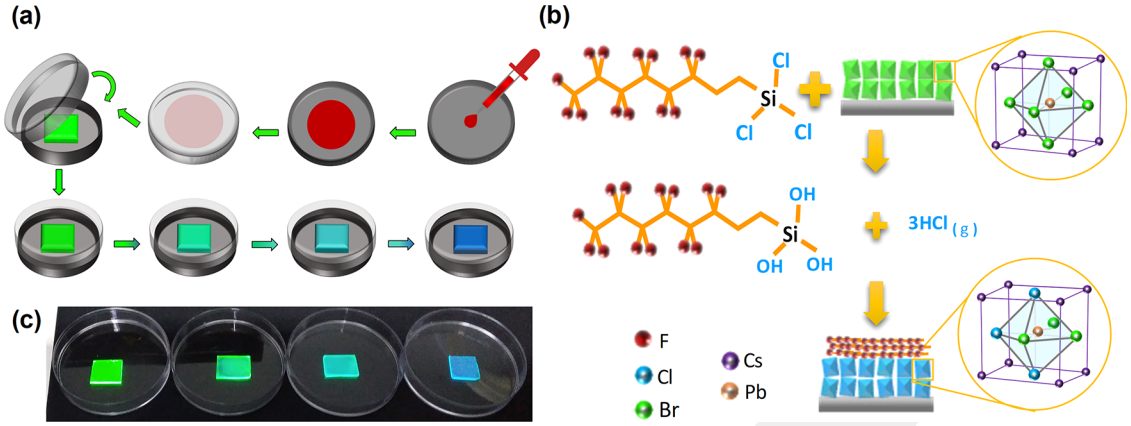

Figure 1. Solid-state encapsulation of PNC films. (a) Schematic description of the process. A droplet of FAS is placed and spread over the entire cover of a Petri dish. The cover is closed on top of a substrate with a film of $CsPbBr_3$ nanocrystals. (b) Schematic illustration of the evolution of the chemical and crystal structure of PNCs and FAS. The composition of $CsPbBr_3$ nanocrystal films shifts to $CsPbBr_{3-x}Cl_x$ with an extent that depends on the duration of FAS deposition and thickness of the PNC film. (c) Photograph of substrates with films of PNCs that were subjected to vapor of FAS for increasing durations.

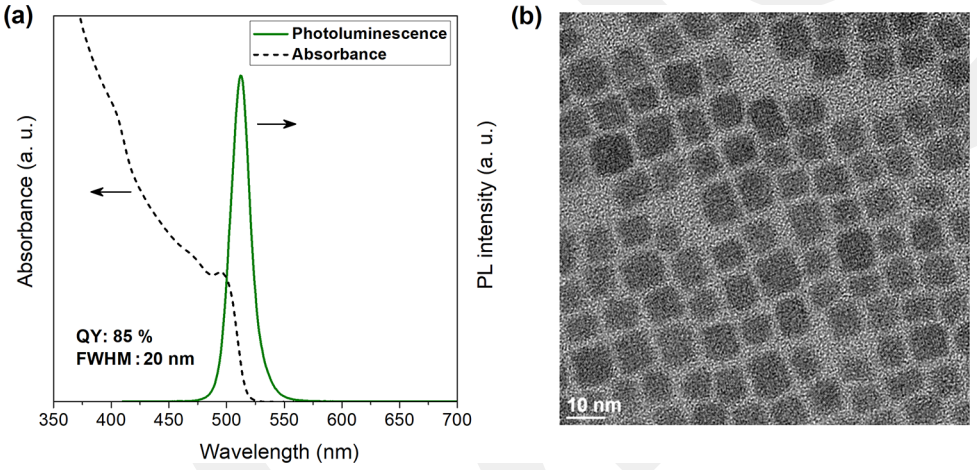

Figure 2. Characterization of PNCs: (a) photoluminescence (PL) and absorbance spectra, (b) TEM image of the synthesized PNCs.

with nitrogen and subjecting to UV-ozone treatment (Bioforce, procleaner) for 20 min.

The substrates were positioned on the bottom of a polystyrene Petri dish (60 mm diameter, 15 mm height). FAS was stored in a glovebox filled with argon, and an aliquot was taken from the glovebox prior to the deposition. A droplet of FAS with a volume of 10 μL was then spread on the cover of the Petri dish and placed 1.35 cm above the substrate, resulting in a closed system in ambient conditions. The deposition was terminated by removing the substrate from the Petri dish.

2.5. Characterization. The wetting property of the substrates was characterized via static water contact angle measurements (Attension Theta Lite system). The volume of the water droplets was fixed as 3 μL. The reported contact angles represent the arithmetic average of at least three measurements performed at different positions of a substrate. The thickness of the deposited films of FAS was measured using a Stokes ellipsometer (Gaertner). On silicon substrates the film was modeled as a substrate (refractive index of 3.85)/native silicon oxide layer (thickness of 1.5 nm, refractive index of 1.543)/FAS (refractive index of 1.35). In the case of gold films vapor deposited on the silicon substrate, the model consisted of a substrate (refractive index of 3.85)/native silicon oxide layer (thickness of 1.5 nm, refractive index of 1.543)/gold film (thickness of 100 nm, refractive index of 0.155)/FAS (refractive index of 1.35). Fourier transform infrared spectroscopy (FTIR) was performed using a spectrophotometer (Thermo Scientific, Nicolet 6700). The topography of the substrates was imaged via an AFM (Veeco Multimode 8). The chemical composition of the substrates was probed by energy-dispersive X-ray (EDX) spectroscopy (Bruker) attached to a SEM (Zeiss EVO LS10). Photoluminescence and absorbance spectra of the PNCs were measured using an Agilent-Cary Eclipse fluorescence spectrophotometer and a Thermo Genesys 10S spectrometer, respectively. Transmission electron microscopy (TEM) images were recorded using a FEI Tecnai G2 F30 microscope. X-ray diffraction measurements were performed with PANalytical: X'pert Pro MPD. The X-ray photoelectron spectroscopy (XPS) analysis was done using a Thermo Scientific K-Alpha X-ray photoelectron spectrometer system.

3. RESULTS AND DISCUSSION

Figure 1a illustrates steps for simultaneous encapsulation and color tuning of films of PNCs by exposure to vapors of FAS. Our approach is based on simple glassware and does not require any kind of special tools. A droplet (~10 μL/cm^2) of FAS is directly placed on top of the cover of a Petri dish. Closing this cover on top of a Petri dish for 10 s is sufficient for vapor-phase deposition of FAS on the surfaces of substrates placed on the bottom of the Petri dish. In the case of the substrates with films of green-emitting $CsPbBr_3$ nanocrystals, the deposition of FAS is accompanied by the blue shift of the color (see Supporting Information Video SV1). We hypothe-

DOI: 10.1021/acsanm.8b02030
ACS Appl. Nano Mater. 2019, 2, 1185−1193

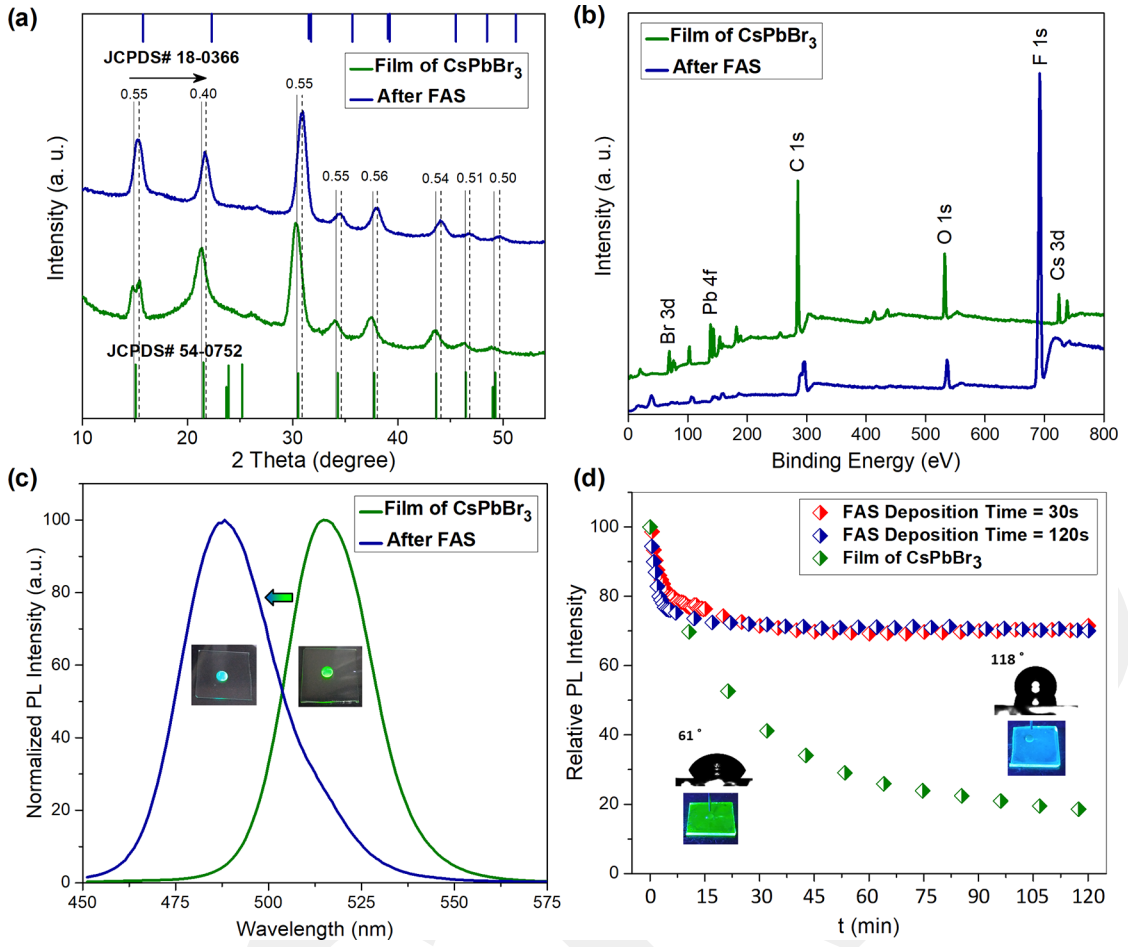

Figure 3. Effect of FAS deposition on the crystal structure, composition, photoluminescence, and water stability of PNC films. (a) XRD and (b) XPS spectra of PNC films before and after FAS deposition. (c) Photoluminescence spectra of the film of $CsPbBr_3$ before and after deposition of FAS. (d) Water stability of PNCs films with and without FAS deposition. The variation of the PL intensity as a function of time that the film of PNCs was subjected to water droplets. The deposition of FAS was performed in air for (a–c) 60 s.

size that such color change is due to the release of hydrochloric acid during the self-hydrolysis of FAS molecules (Figure 1b). Previous reports[23,31,32] have shown that exposure of the films of perovskites to hydrohalic vapors result in the exchange of anions. For the results shown here, the partial exchange of Br anions with Cl anions occurs with the exposure to FAS. Such anion-exchange results in the blue shift of the emission color (Figure 1c). Simultaneously, FAS molecules are deposited on top of the films of PNCs constituting a hydrophobic encapsulation layer.

The strength of our approach is that high-performance colloidal PNCs can be directly used without intervening with the synthesis process. We used the colloidal synthesis method originally described by Kovalenko and co-workers.[5] The green (centered at 514 nm) emissive PNCs exhibited high color purity with a quantum yield of 85% and a full width at half-maximum (FWHM) of 20 nm (Figure 2a). The TEM image presented in Figure 2b shows that the average length and width of the PNCs were 9.31 ± 0.89 nm and 8.05 ± 0.97 nm, respectively. The crystal structure of PNCs can vary in between orthorhombic, tetragonal, and cubic, depending on the synthesis and injection temperature of the chemicals for the nucleation.[35] In this study, synthesis of PNCs at 180 °C led to the cubic perovskite structure, which is typically observed at high temperatures.[5,35]

Figure 3 summarizes the impact of FAS deposition on the characteristics of PNC films. The XRD, XPS, photoluminescence, and water stability of the films of PNCs were investigated before and after deposition of FAS. The XRD spectrum (Figure 3a) of the as-synthesized and FAS deposited PNCs presented peaks that are well coincident with the cubic perovskite crystal structure of the $CsPbBr_3$ (JCPDS: 54-0752) and $CsPbCl_3$ (JCPDS: 18-0366) as reported in previous studies.[5,35,36] The XPS spectrum (Figure 3b) showed the presence of Cs, Pb, Br, C, and O elements, which constitute the nanocrystal and its ligands. The vapor-phase deposition of FAS was clearly evident in the XPS and XRD analysis. The XRD spectrum of the PNCs shifted to higher angles due to the exchange of anions from Br to Cl during the deposition of FAS. This shift is due to the shrinkage of the cell with the incorporation of smaller size Cl atoms as reported in previous studies.[5,30] A strong F 1s peak appeared in the XPS analysis confirming the deposition of a layer of FAS molecules. The decrease in the intensity of other elements further supports deposition of a film that covers the surface of the substrate, since XPS is a surface-sensitive technique with a depth of penetration about 5 nm. EDX analysis further supported the simultaneous partial anion exchange and deposition of FAS on the PNC films (see Supporting Information Figure S1). A distinct Cl peak appeared following deposition of FAS, and the

DOI: 10.1021/acsanm.8b02030
ACS Appl. Nano Mater. 2019, 2, 1185–1193

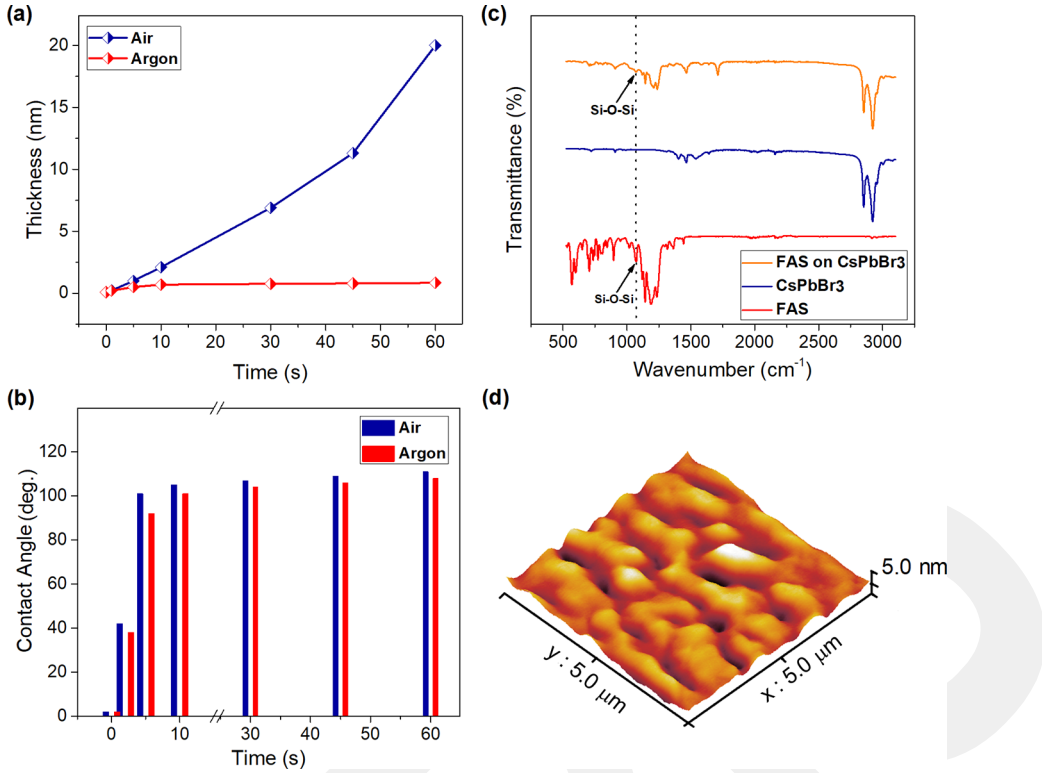

Figure 4. Vapor-phase deposition of FAS. (a) The thickness and (b) water contact angle of the films of vapor-deposited FAS as a function of time in air and argon atmospheres. (c) FTIR characterization of FAS, $CsPbBr_3$ and FAS deposited on $CsPbBr_3$. (d) AFM image of a silicon substrate following vapor-phase deposition of FAS for 20 s.

ratio of Br:Cl decreased with increasing deposition time of FAS. The morphology of the film of PNCs remained mostly the same after the deposition of FAS (see Figure S2).

The exposure to vapor of FAS resulted in alteration of the surface wetting and photoluminescence properties of films of PNCs. Initially the surface of the film of PNCs was hydrophilic (~61°) due to the polar nature of the material. The rapid degradation of PNCs upon contact with water prevented accurate measurement of the water contact angle. FAS is a well-known fluorocarbon material that provides low surface energy and commonly employed in fabrication of extremely water-repellant surfaces.[37] After vapor-phase deposition of FAS, the surface became hydrophobic with a water contact angle of 118°. Along with the change in the wettability, the emission peak wavelength of the PNC film shifted from green to blue with exposure to FAS vapor (Figure 3c). The quantum efficiencies (see Supporting Information and Figure S3 for details) were 44.6% and 28.5% for the uncoated and FAS deposited films of PNCs, respectively. The extent of the blue shift depended on the duration of the exposure to FAS vapor and thickness of the PNC film. For spin-coated films of $CsPbBr_3$ nanocrystals, the emission peak wavelength decreased with increasing duration of the exposure to FAS vapor (see Figure S4). For films deposited by drop-casting of $CsPbBr_3$ nanocrystals on the hydrophobized substrate, the blue shift of the photoluminescence started with the deposition of FAS and continued for a period of time following termination of the FAS deposition process (see Figure S5). The penetration and rearrangement of atoms in the relatively thick stacks of PNCs deposited by drop-casting can be responsible for the progression of the blue-shift following termination of the FAS deposition. This kind of blue-shift in the emission of films of all inorganic PNCs was previously observed in response to exposure to vapors of hydrochloric acid.[23,31] Together with the spectroscopic analysis presented above, these results strongly suggest that a similar partial anion exchange from Br to Cl occurs in this study.

We further studied the stability of PNC films upon encapsulation. The low surface energy provided by FAS acts as an effective barrier against penetration of water molecules to the film of PNCs. To demonstrate the stability of the PNCs, we set up a spectrometer based measurement system to track the emission intensity of drop-casted samples excited with a blue LED. A dispersion of green-emitting $CsPbBr_3$ PNCs in hexane with a volume of 20 μL was drop-casted on two glass substrates. One of the glass substrates with the film of PNCs was subjected to the vapor of FAS for 10 s, whereas the other substrate was not subjected to any additional processing. Several droplets of deionized water were spotted on the both substrates following the record of initial spectrum under the spectrometer. The relative peak intensities calculated from the periodically recorded spectra are shown in Figure 3d. While the photoluminescence degradation of the uncoated substrate was up to 80% in 120 min, the coated substrate lost only 30% of the initial intensity. The water stability behavior was similar for varying FAS deposition times. The deposition of FAS also resulted in an improvement in the air stability of the films of PNCs (see Figure S6). Control experiments performed with vapor of hydrochloric acid instead of FAS did not result in significant improvement in the stability of PNC films. This difference in the stability is attributed to the low surface energy film provided by FAS. The enhancement of the stability can be related to the surface state of PNCs as determined with the interaction with FAS molecules.[17,27,38] In the absence of FAS,

DOI: 10.1021/acsanm.8b02030
ACS Appl. Nano Mater. 2019, 2, 1185−1193

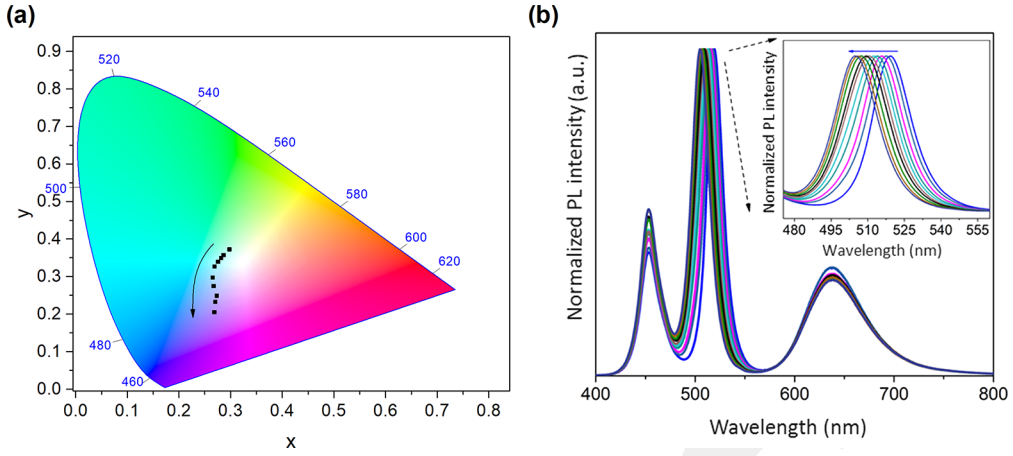

Figure 5. Use of solid-state color change in the modulation of (a) CIE color coordinates and (b) obtained white LED spectrum. The inset in (b) shows the shift in PL emission of the PNCs during the FAS deposition.

the integrity of PNCs is lost upon contact with water, resulting in the degradation of the photoluminescence.[39]

To understand the origin of the deposition of a hydrophobic layer on the films of PNCs, we investigated the deposition of FAS using different atmospheres, times, and substrates. The vapor-phase deposition of FAS was performed for different times on a freshly cleaned silicon substrate in air and argon gas atmospheres. We measured the thickness (Figure 4a) and water contact angle (Figure 4b) of the deposited films of FAS. The deposition of FAS was much faster in air than an argon atmosphere. The thickness of the film increased with the duration of the deposition. After 60 s of the deposition, the thickness of the FAS film was ∼20 nm in air, whereas it was <2 nm in an argon atmosphere. The strong contrast in the thickness of the films that were deposited in air and argon atmospheres was attributed to the effect of water for the rapid deposition of FAS molecules. Previous studies have shown the importance of moisture on the deposition of silane molecules. In the presence of water, trichlorosilanes are hydrolyzed to silanols with hydrochloric acid as the byproduct of this reaction.[40,41] The hydrolysis is followed by reaction between the individual silanes to form oligomers (i.e., self-polymerization), which are then condensed to form a nonvolatile and hydrophobic layer on the substrate. The oligomers adsorb to the surfaces more rapidly than their single silane counterparts. The rate of adsorption has been reported to increase with increasing concentration of water.[42] Fluorinated trichlorosilanes were reported to be more reactive to water and easier to self-polymerize in comparison with their hydrogenated counterparts.[43,44] The deposition of thick layers of FAS in ambient atmosphere is likely a result of the rapid self-polymerization of FAS to form a polysiloxane layer. The deposition of such a hydrophobic layer as a result of hydrolysis followed by self-polymerization may play a critical role in the improved water stability of PNC films. The absence of water molecules in the controlled argon atmosphere limits the hydrolysis reaction. Despite a strong contrast in the thickness of the films, the water contact angles of the substrates prepared in air and argon did not show a significant difference (Figure 4b). This result implies that a thin layer of FAS is sufficient to alter the wetting properties of the substrates. The infrared absorption spectra clearly showed the presence of vibrations due to Si−O−Si bands at ∼1143 cm^{-1} on FAS films deposited on the PNCs (Figure 4c). The presence of Si−O−Si bands suggests that FAS molecules oligomerize in the vapor phase followed by condensation to form siloxane linkages. The formation of siloxane linkages may further contribute to the stability of films of PNCs.[17]

To further probe the vapor-phase deposition of FAS on the films of PNCs, we performed experiments using gold-coated silicon substrates. The study of FAS deposition process on gold-coated substrates was important for two different reasons. First, gold-coated substrates allowed us to study the FAS deposition process on a surface that is orthogonal to silicon oxide-terminated surfaces. FAS is known to react and chemically bind to silicon oxide-terminated substrates.[40,45] To show that our processing conditions lead to deposition of FAS molecules on a surface without any chemical binding sites, we performed experiments with gold-coated substrates. Gold presents an orthogonal chemistry and does not have any chemical binding sites for bond formation with silanes.[46] Second, the gold-coated silicon substrates enabled comparison of the deposition rate of FAS on different substrates. A 100 nm film of gold was vapor deposited on a silicon substrate. The gold-coated and bare silicon substrates were subjected to vapor-phase deposition of FAS for 30 s. Both substrates became hydrophobic with a water contact angle of ∼110° and a FAS thickness of ∼7.5 nm (see Table S1). The rate of deposition of FAS was similar on silicon and gold-coated silicon substrates. This result suggests that the rate of FAS deposition does not depend on the surface chemistry of the substrate and can be expected to be similar on films of PNCs. Si−O−Si bonds could be observed on the gold-coated silicon substrate, suggesting the self-polymerization of FAS to form siloxane layers (Figure S7). The vapor-phase deposition of such siloxane layers was reported on organic semiconductor layers that are different than the silicon oxide surfaces, which can react with silanes.[47,48] Washing the gold coated and bare silicon substrates for 2 min under sonication with water showed a strong contrast in between the substrates. The silicon substrate was still hydrophobic (θ = 109°), whereas the gold-coated silicon substrate became hydrophilic (θ = 60°). The thickness of the FAS film reduced to 2.3 nm on the silicon substrate, and there was no discernible layer on the gold-coated silicon substrate. These results show that vapor-phase deposition of FAS results in a physically bound layer on the gold surface. The absence of suitable binding sites on the films of PNCs suggests the formation of a similar layer of FAS. AFM

DOI: 10.1021/acsanm.8b02030
ACS Appl. Nano Mater. 2019, 2, 1185−1193

images (Figure 4d) of the silicon substrate after the deposition of FAS further show formation of a highly rough layer, which is typical for polymerization of silanes in the presence of water.[40,47]

The color tunability of the green emitting PNCs by FAS coating was demonstrated by shifting the coordinate of the white light generated by the hybridized structure of green-emitting $CsPbBr_3$, red emitting InP/ZnS quantum dots, and commercially available blue LED (see the Supporting Information for details). InP-based red-emitting quantum dots (QDs) were synthesized according to the previous studies.[49,50] The peak wavelength of the green emitting QDs was shifted by FAS deposition with the aforementioned procedure. It is worth noting here that the FAS has not affected the emission of the InP-based red-emitting QDs, as expected. To investigate the coordinate shift of the hybrid device, the FAS amount and exposure time were reduced to 2 μL and 3 s, respectively. The progressive shift of the white coordinates on the CIE diagram and the PL spectrum is shown in Figure 5a,b, and the x, y values are tabulated in Table S2. The chromaticity coordinates were calculated using the spectral power distribution of the light and CIE color matching functions (see the Supporting Information for details). The (x, y) coordinates of a light are a widely accepted quality parameter, especially for white light. Depending on the specific requirements of application area, various white lights with different correlated color temperatures (CCT) are used.[51] While the yellowish-white light is believed to be more soothing, blueish-white light is suggested for office spaces where concentration is more important. Apart from ordinary lighting solutions, CCT plays an important role in some niche applications such as jewelry displays, museum and gallery lighting, and so forth. Although conventional color tunability is performed by choosing the appropriate nanocrystals of different fixed emission profile (fixing green and red emitters), in our work, we demonstrate a coordinate shift by using vapor deposition on color converting agents in real time. As the continuous tunability[52] of the color coordinates is an enabling capability for varying needs of different applications, in this respect, the engineering of the color coordinates in an on-chip, real-time approach via a simple process to span the white region is a new and alternative approach which cannot be performed by other solution-processable methods.

4. CONCLUSIONS

This study demonstrated the promise of solid-state encapsulation of films of nanoscale crystals of perovskites through vapor-phase deposition of fluorinated silane molecules and fabricated white-light-emitting diodes with engineered color coordinates through the color shift initiated by anion exchange of the PNCs. The strength of our approach emerges from the simplicity of the vapor-phase deposition together with the solid-state encapsulation of the films. Our approach enables postfabrication encapsulation of the light-emitting diodes of varying geometry, planarity, and area and allows for retainment of the materials and processing steps optimized for high performance (e.g., high quantum yield). We anticipate that with slight modifications, this approach can be easily adapted for films of perovskites in photovoltaic applications. The presented results motivate development of materials and processes for solid-state encapsulation of light-emitting devices.

■ ASSOCIATED CONTENT

Supporting Information

The Supporting Information is available free of charge on the ACS Publications website at DOI: 10.1021/acsanm.8b02030.

Synthesis of InP-based red-emitting quantum dots, calculation of quantum efficiency, fabrication of WLED, energy-dispersive X-ray (EDX) spectroscopy analysis, FTIR analysis, SEM images, air-stability results, effect of FAS deposition time on the color shift, thickness and water contact angles on gold-coated silicon substrates, color coordinates of the WLED (PDF)

Vapor-phase deposition of FAS and color tunability (MPG)

■ AUTHOR INFORMATION

Corresponding Authors

*E-mail onses@erciyes.edu.tr (M.S.O.).
*E-mail evren.mutlugun@agu.edu.tr (E.M.).

ORCID

Evren Mutlugun: 0000-0003-3715-5594
M. Serdar Onses: 0000-0001-6898-7700

Notes

The authors declare no competing financial interest.

■ ACKNOWLEDGMENTS

M.S.O. and E.M. acknowledge TUBITAK project no. 117E239 and Turkish Academy of Sciences Distinguished Young Scientist Award (TUBA-GEBIP).

■ REFERENCES

(1) Akkerman, Q. A.; Raino, G.; Kovalenko, M. V.; Manna, L. Genesis, Challenges and Opportunities for Colloidal Lead Halide Perovskite Nanocrystals. *Nat. Mater.* **2018**, *17*, 394−405.

(2) Green, M. A.; Ho-Baillie, A.; Snaith, H. J. The Emergence of Perovskite Solar Cells. *Nat. Photonics* **2014**, *8*, 506−514.

(3) Schmidt, L. C.; Pertegas, A.; González-Carrero, S.; Malinkiewicz, O.; Agouram, S.; Minguez Espallargas, G.; Bolink, H. J.; Galian, R. E.; Perez-Prieto, J. Nontemplate Synthesis of CH3NH3PbBr3 Perovskite Nanoparticles. *J. Am. Chem. Soc.* **2014**, *136*, 850−853.

(4) Huang, H.; Susha, A. S.; Kershaw, S. V.; Hung, T. F.; Rogach, A. L. Control of Emission Color of High Quantum Yield CH3NH3PbBr3 Perovskite Quantum Dots by Precipitation Temperature. *Adv. Sci.* **2015**, *2*, 1500194.

(5) Protesescu, L.; Yakunin, S.; Bodnarchuk, M. I.; Krieg, F.; Caputo, R.; Hendon, C. H.; Yang, R. X.; Walsh, A.; Kovalenko, M. V. Nanocrystals of Cesium Lead Halide Perovskites (CsPbX3, X= Cl, Br, and I): Novel Optoelectronic Materials Showing Bright Emission With Wide Color Gamut. *Nano Lett.* **2015**, *15*, 3692−3696.

(6) Song, J.; Li, J.; Li, X.; Xu, L.; Dong, Y.; Zeng, H. Quantum Dot Light-Emitting Diodes Based on Inorganic Perovskite Cesium Lead Halides (CsPbX3). *Adv. Mater.* **2015**, *27*, 7162−7167.

(7) Kim, Y.-H.; Wolf, C.; Kim, Y.-T.; Cho, H.; Kwon, W.; Do, S.; Sadhanala, A.; Park, C. G.; Rhee, S.-W.; Im, S. H.; Friend, R. H.; Lee, T.-W. Highly Efficient Light-Emitting Diodes of Colloidal Metal−Halide Perovskite Nanocrystals Beyond Quantum Size. *ACS Nano* **2017**, *11*, 6586−6593.

(8) Chen, M.; Zou, Y.; Wu, L.; Pan, Q.; Yang, D.; Hu, H.; Tan, Y.; Zhong, Q.; Xu, Y.; Liu, H.; Sun, B.; Zhang, Q. Solvothermal Synthesis of High-Quality All-Inorganic Cesium Lead Halide Perovskite Nanocrystals: From Nanocube to Ultrathin Nanowire. *Adv. Funct. Mater.* **2017**, *27*, 1701121.

(9) Wang, Y.; Li, X.; Zhao, X.; Xiao, L.; Zeng, H.; Sun, H. Nonlinear Absorption and Low-Threshold Multiphoton Pumped Stimulated

DOI: 10.1021/acsanm.8b02030
ACS Appl. Nano Mater. 2019, 2, 1185−1193

Emission from All-inorganic Perovskite Nanocrystals. *Nano Lett.* **2016**, *16*, 448−453.
(10) Dirin, D. N.; Protesescu, L.; Trummer, D.; Kochetygov, I. V.; Yakunin, S.; Krumeich, F.; Stadie, N. P.; Kovalenko, M. V. Harnessing Defect-Tolerance at the Nanoscale: Highly Luminescent Lead Halide Perovskite Nanocrystals in Mesoporous Silica Matrixes. *Nano Lett.* **2016**, *16*, 5866−5874.
(11) Wang, L.; Liu, B.; Zhao, X.; Demir, H. V.; Gu, H.; Sun, H. Solvent-Assisted Surface Engineering for High Performance All-Inorganic Perovskite Naanocrystals Light-Emitting Diodes. *ACS Appl. Mater. Interfaces* **2018**, *10*, 19828−19835.
(12) Wang, Y.; Li, X.; Song, J.; Xiao, L.; Zeng, H.; Sun, H. All-Inorganic Colloidal Perovskite Quantum Dots: A New Class of Lasing Materials with Favorable Characteristics. *Adv. Mater.* **2015**, *27*, 7101−7108.
(13) Akkerman, Q. A.; Gandini, M.; Di Stasio, F.; Rastogi, P.; Palazon, F.; Bertoni, G.; Ball, J. M.; Prato, M.; Petrozza, A.; Manna, L. Strongly Emissive Perovskite Nanocrystal Inks for High-Voltage Solar Cells. *Nat. Energy* **2017**, *2*, 16194.
(14) Ramasamy, P.; Lim, D.-H.; Kim, B.; Lee, S.-H.; Lee, M.-S.; Lee, J.-S. All-Inorganic Cesium Lead Halide Perovskite Nanocrystals for Photodetector Applications. *Chem. Commun.* **2016**, *52*, 2067−2070.
(15) Huang, H.; Bodnarchuk, M. I.; Kershaw, S. V.; Kovalenko, M. V.; Rogach, A. L. Lead Halide Perovskite Nanocrystals in the Research Spotlight: Stability and Defect Tolerance. *ACS Energy Lett.* **2017**, *2*, 2071−2083.
(16) Huang, H.; Chen, B.; Wang, Z.; Hung, T. F.; Susha, A. S.; Zhong, H.; Rogach, A. L. Water Resistant CsPbX3 Nanocrystals Coated With Polyhedral Oligomeric Silsesquioxane and Their Use as Solid State Luminophores in All-Perovskite White Light-Emitting Devices. *Chem. Sci.* **2016**, *7*, 5699−5703.
(17) Sun, C.; Zhang, Y.; Ruan, C.; Yin, C.; Wang, X.; Wang, Y.; Yu, W. W. Efficient and Stable White LEDs with Silica-Coated Inorganic Perovskite Quantum Dots. *Adv. Mater.* **2016**, *28*, 10088−10094.
(18) Xu, L.; Chen, J.; Song, J.; Li, J.; Xue, J.; Dong, Y.; Cai, B.; Shan, Q.; Han, B.; Zeng, H. Double-Protected All-Inorganic Perovskite Nanocrystals by Crystalline Matrix and Silica for Triple-Modal Anti-Counterfeiting Codes. *ACS Appl. Mater. Interfaces* **2017**, *9*, 26556−26564.
(19) Hai, J.; Li, H.; Zhao, Y.; Chen, F.; Peng, Y.; Wang, B. Designing of Blue, Green, and Red CsPbX3 Perovskite-Codoped Flexible Films With Water Resistant Property and Elimination of Anion-Exchange for Tunable White Light Emission. *Chem. Commun.* **2017**, *53*, 5400−5403.
(20) Raja, S. N.; Bekenstein, Y.; Koc, M. A.; Fischer, S.; Zhang, D.; Lin, L.; Ritchie, R. O.; Yang, P.; Alivisatos, A. P. Encapsulation of Perovskite Nanocrystals into Macroscale Polymer Matrices: Enhanced Stability and Polarization. *ACS Appl. Mater. Interfaces* **2016**, *8*, 35523−35533.
(21) Hou, S.; Guo, Y.; Tang, Y.; Quan, Q. Synthesis and Stabilization of Colloidal Perovskite Nanocrystals by Multidentate Polymer Micelles. *ACS Appl. Mater. Interfaces* **2017**, *9*, 18417−18422.
(22) Zhang, H.; Wang, X.; Liao, Q.; Xu, Z.; Li, H.; Zheng, L.; Fu, H. Embedding Perovskite Nanocrystals into a Polymer Matrix for Tunable Luminescence Probes in Cell Imaging. *Adv. Funct. Mater.* **2017**, *27*, 1604382.
(23) Palazon, F.; Akkerman, Q. A.; Prato, M.; Manna, L. X-ray Lithography on Perovskite Nanocrystals Films: From Patterning With Anion-Exchange Reactions to Enhanced Stability in Air and Water. *ACS Nano* **2016**, *10*, 1224−1230.
(24) Wang, H. C.; Lin, S. Y.; Tang, A. C.; Singh, B. P.; Tong, H. C.; Chen, C. Y.; Lee, Y. C.; Tsai, T. L.; Liu, R. S. Mesoporous Silica Particles Integrated with All-Inorganic CsPbBr3 Perovskite Quantum-Dot Nanocomposites (MP-PQDs) with High Stability and Wide Color Gamut Used for Backlight Display. *Angew. Chem., Int. Ed.* **2016**, *55*, 7924−7929.
(25) Li, X.; Wang, Y.; Sun, H.; Zeng, H. Amino-Mediated Anchoring Perovskite Quantum Dots for Stable and Low-Threshold Random Lasing. *Adv. Mater.* **2017**, *29*, 1701185.
(26) Jing, Q.; Zhang, M.; Huang, X.; Ren, X.; Wang, P.; Lu, Z. Surface Passivation of Mixed-Halide Perovskite CsPb (Br x I 1− x) 3 Nanocrystals by Selective Etching for Improved Stability. *Nanoscale* **2017**, *9*, 7391−7396.
(27) Chen, W.; Hao, J.; Hu, W.; Zang, Z.; Tang, X.; Fang, L.; Niu, T.; Zhou, M. Enhanced Stability and Tunable Photoluminescence in Perovskite CsPbX3/ZnS Quantum Dot Heterostructure. *Small* **2017**, *13*, 1604085.
(28) Wang, C.; Chesman, A. S.; Jasieniak, J. J. Stabilizing the Cubic Perovskite Phase of CsPbI3 Nanocrystals by Using an Alkyl Phosphinic Acid. *Chem. Commun.* **2017**, *53*, 232−235.
(29) Nedelcu, G.; Protesescu, L.; Yakunin, S.; Bodnarchuk, M. I.; Grotevent, M. J.; Kovalenko, M. V. Fast Anion-Exchange in Highly Luminescent Nanocrystals of Cesium Lead Halide Perovskites (CsPbX3, X= Cl, Br, I). *Nano Lett.* **2015**, *15*, 5635−5640.
(30) Akkerman, Q. A.; D'Innocenzo, V.; Accornero, S.; Scarpellini, A.; Petrozza, A.; Prato, M.; Manna, L. Tuning the Optical Properties of Cesium Lead Halide Perovskite Nanocrystals by Anion Exchange Reactions. *J. Am. Chem. Soc.* **2015**, *137*, 10276−10281.
(31) Chen, X.; Hu, H.; Xia, Z.; Gao, W.; Gou, W.; Qu, Y.; Ma, Y. CsPbBr3 Perovskite Nanocrystals as Highly Selective and Sensitive Spectrochemical Probes for Gaseous HCl Detection. *J. Mater. Chem. C* **2017**, *5*, 309−313.
(32) Zhou, W.; Zhou, P.; Lei, X.; Fang, Z.; Zhang, M.; Liu, Q.; Chen, T.; Zeng, H.; Ding, L.; Zhu, J.; Dai, S.; Yang, S. Phase Engineering of Perovskite Materials for High-efficiency Solar Cells: Rapid Conversion of $CH_3NH_3PbI_3$ to Phase-Pure $CH_3NH_3PbCl_3$ via Hydrochloric Acid Vapor Annealing Post-Treatment. *ACS Appl. Mater. Interfaces* **2018**, *10*, 1897−1908.
(33) De Roo, J.; Ibáñez, M.; Geiregat, P.; Nedelcu, G.; Walravens, W.; Maes, J.; Martins, J. C.; Van Driessche, I.; Kovalenko, M. V.; Hens, Z. Highly Dynamic Ligand Binding and Light Absorption Coefficient of Cesium Lead Bromide Perovskite Nanocrystals. *ACS Nano* **2016**, *10*, 2071−2081.
(34) Dadı, S.; Altıntas, Y.; Beskazak, E.; Mutlugun, E. Plasmon Enhanced Emission of Perovskite Quantum Dot Films. *MRS Advances* **2018**, *3*, 733−739.
(35) Tang, X.; Hu, Z.; Chen, W.; Xing, X.; Zang, Z.; Hu, W.; Qiu, J.; Du, J.; Leng, Y.; Jiang, X.; Mai, L. Room Temperature Single-Photon Emission and Lasing for All-Inorganic Colloidal Perovskite Quantum Dots. *Nano Energy* **2016**, *28*, 462−468.
(36) Zhang, M.; Wang, M.; Yang, Z.; Li, J.; Qiu, H. Preparation of All-Inorganic Perovskite Quantum Dots-Polymer Composite for White LEDs Application. *J. Alloys Compd.* **2018**, *748*, 537−545.
(37) Torun, I.; Onses, M. S. Robust Superhydrophobicity on Paper: Protection of Spray-Coated Nanoparticles Against Mechanical Wear by the Microstructure of Paper. *Surf. Coat. Technol.* **2017**, *319*, 301−308.
(38) Xiao, G.; Cao, Y.; Qi, G.; Wang, L.; Liu, C.; Ma, Z.; Yang, X.; Sui, Y.; Zheng, W.; Zou, B. Pressure Effects on Structure and Optical Properties in Cesium Lead Bromide Perovskite Nanocrystals. *J. Am. Chem. Soc.* **2017**, *139*, 10087−10094.
(39) Cao, Y.; Qi, G.; Liu, C.; Wang, L.; Ma, Z.; Wang, K.; Du, F.; Xiao, G.; Zou, B. Pressure-Tailored Band Gap Engineering and Structure Evolution of Cubic Cesium Lead Iodide Perovskite Nanocrystals. *J. Phys. Chem. C* **2018**, *122*, 9332−9338.
(40) Jung, G.-Y.; Li, Z.; Wu, W.; Chen, Y.; Olynick, D. L.; Wang, S.-Y.; Tong, W. M.; Williams, R. S. Vapor-Phase Self-Assembled Monolayer for Improved Mold Release in Nanoimprint Lithography. *Langmuir* **2005**, *21*, 1158−1161.
(41) Zhuang, Y. X.; Hansen, O.; Knieling, T.; Wang, C.; Rombach, P.; Lang, W.; Benecke, W.; Kehlenbeck, M.; Koblitz, J. Vapor-Phase Self-Assembled Monolayers for Anti-Stiction Applications in MEMS. *J. Microelectromech. Syst.* **2007**, *16*, 1451−1460.
(42) Peters, R. D.; Nealey, P. F.; Crain, J. N.; Himpsel, F. J. A Near Edge X-ray Absorption Fine Structure Spectroscopy Investigation of the Structure of Self-Assembled Films of Octadecyltrichlorosilane. *Langmuir* **2002**, *18*, 1250−1256.

DOI: 10.1021/acsanm.8b02030
ACS Appl. Nano Mater. 2019, 2, 1185−1193

(43) Brzoska, J.; Azouz, I. B.; Rondelez, F. Silanization of Solid Substrates: A Step Toward Reproducibility. *Langmuir* **1994**, *10*, 4367−4373.
(44) Tripp, C.; Veregin, R.; Hair, M. Effect of Fluoroalkyl Substituents on the Reaction of Alkylchlorosilanes with Silica Surfaces. *Langmuir* **1993**, *9*, 3518−3522.
(45) Torun, I.; Celik, N.; Hancer, M.; Es, F.; Emir, C.; Turan, R. i.; Onses, M. S. Water Impact Resistant and Antireflective Superhydrophobic Surfaces Fabricated by Spray Coating of Nanoparticles: Interface Engineering via End-Grafted Polymers. *Macromolecules* **2018**, *51*, 10011−10020.
(46) Schenk, F. C.; Boehm, H.; Spatz, J. P.; Wegner, S. V. Dual-Functionalized Nanostructured Biointerfaces by Click Chemistry. *Langmuir* **2014**, *30*, 6897−6905.
(47) Kao, C. Y.; Lee, B.; Wielunski, L. S.; Heeney, M.; McCulloch, I.; Garfunkel, E.; Feldman, L. C.; Podzorov, V. Doping of Conjugated Polythiophenes With Alkyl Silanes. *Adv. Funct. Mater.* **2009**, *19*, 1906−1911.
(48) Calhoun, M.; Sanchez, J.; Olaya, D.; Gershenson, M.; Podzorov, V. Electronic Functionalization of the Surface of Organic Semiconductors With Self-Assembled Monolayers. *Nat. Mater.* **2008**, *7*, 84−89.
(49) Tessier, M. D.; Dupont, D.; De Nolf, K.; De Roo, J.; Hens, Z. Economic and Size-Tunable Synthesis of InP/ZnE (E= S, Se) Colloidal Quantum Dots. *Chem. Mater.* **2015**, *27*, 4893−4898.
(50) Altıntas, Y.; Talpur, M. Y.; Mutlugün, E. Efficient Förster Resonance Energy Transfer Donors of In (Zn) P/ZnS Quantum Dots. *J. Phys. Chem. C* **2017**, *121*, 3034−3043.
(51) Altıntas, Y.; Kiremitler, N. B.; Genç, S.; Onses, M. S.; Mutlugün, E. FRET Enabled Light Harvesting Within Quantum Dot Loaded Nanofibers. *J. Phys. D: Appl. Phys.* **2018**, *51*, 065111.
(52) Ma, Z.; Liu, Z.; Lu, S.; Wang, L.; Feng, X.; Yang, D.; Wang, K.; Xiao, G.; Zhang, L.; Redfern, S. A.; Zou, B. Pressure-Induced Emission of Cesium Lead Halide Perovskite Nanocrystals. *Nat. Commun.* **2018**, *9*, 4506.

DOI: 10.1021/acsanm.8b02030
ACS Appl. Nano Mater. 2019, 2, 1185−1193